ARL

US Army Research Laboratory

Modeling Ballistic Response of Ultra-High-Molecular-Weight Polyethylene (UHMWPE)

by Timothy G Zhang, Sikhanda S Satapathy, Lionel R Vargas-Gonzalez, and Shawn M Walsh

NOTICES

Disclaimers

The findings in this report are not to be construed as an official Department of the Army position unless so designated by other authorized documents.

Citation of manufacturer's or trade names does not constitute an official endorsement or approval of the use thereof.

Destroy this report when it is no longer needed. Do not return it to the originator.

US Army Research Laboratory

Modeling Ballistic Response of Ultra-High-Molecular-Weight Polyethylene (UHMWPE)

by Timothy G Zhang
TKC Global Inc.

Sikhanda S Satapathy, Lionel R Vargas-Gonzalez, and Shawn M Walsh
Weapons and Materials Research Directorate, ARL

1. REPORT DATE *(DD-MM-YYYY)*	2. REPORT TYPE	3. DATES COVERED (From - To)
July 2016	Final	January–December 2014

4. TITLE AND SUBTITLE	5a. CONTRACT NUMBER
Modeling Ballistic Response of Ultra-High-Molecular-Weight Polyethylene (UHMWPE)	
	5b. GRANT NUMBER
	5c. PROGRAM ELEMENT NUMBER

6. AUTHOR(S)	5d. PROJECT NUMBER
Timothy G Zhang, Sikhanda S Satapathy, Lionel R Vargas-Gonzalez, and Shawn M Walsh	
	5e. TASK NUMBER
	5f. WORK UNIT NUMBER

7. PERFORMING ORGANIZATION NAME(S) AND ADDRESS(ES)	8. PERFORMING ORGANIZATION REPORT NUMBER
US Army Research Laboratory ATTN: RDRL-WMP-B Aberdeen Proving Ground, MD 21005-5069	ARL-TR-7723

9. SPONSORING/MONITORING AGENCY NAME(S) AND ADDRESS(ES)	10. SPONSOR/MONITOR'S ACRONYM(S)
	11. SPONSOR/MONITOR'S REPORT NUMBER(S)

12. DISTRIBUTION/AVAILABILITY STATEMENT

Approved for public release; distribution is unlimited.

13. SUPPLEMENTARY NOTES

14. ABSTRACT

This report presents a numerical model that captures various aspects of ballistic behavior of ultra-high-molecular-weight polyethylene, such as ballistic limit V_{50}, back-face deformation (BFD) profile, remaining thickness of intact material, and interior delamination. The roles of fiber tension/shear and crush failure were investigated using a finite element model. Delamination due to matrix material failure at the interface between adjacent layers was investigated using a tiebreak contact algorithm. Parametric analyses were carried out to identify sensitive parameters that affected the material response to ballistic loading conditions. The results suggest that better helmet material needs to have higher interlaminar tensile strength, transverse Young's modulus, and crush strength and smaller transverse shear modulus and damage softening parameters. The parametric study also indicated that higher in-plane shear modulus resulted in lower V_{50} and lower BFD. A set of material parameters was identified that best fit the V_{50}, BFD profile, remaining thickness of intact composites, and delamination failure observed in the experiments.

15. SUBJECT TERMS

Dyneema HB80, BFD, ballistic limit V_{50}, delamination, tiebreak contact

16. SECURITY CLASSIFICATION OF:			17. LIMITATION OF ABSTRACT	18. NUMBER OF PAGES	19a. NAME OF RESPONSIBLE PERSON
					Timothy G Zhang
a. REPORT	b. ABSTRACT	c. THIS PAGE	UU	46	19b. TELEPHONE NUMBER (Include area code)
Unclassified	Unclassified	Unclassified			410-306-2984

Contents

List of Figures

List of Tables

Preface

The research reported in this document was performed in connection with contract/instrument W911QX-14-C-0016 with the US Army Research Laboratory. The views and conclusions contained in this document are those of TKC Global and the US Army Research Laboratory. Citation of manufacturer's or trade names does not constitute an official endorsement or approval of the use thereof. The US government is authorized to reproduce and distribute reprints for government purposes notwithstanding any copyright notation hereon.

INTENTIONALLY LEFT BLANK.

1.   Introduction

Ultra-high-molecular-weight polyethylene (UHMWPE) composites exhibit excellent ballistic behavior, which makes them ideal for protection applications. While its penetration resistance (V_{50}) is superior, the composite shows significant deformation characterized by bulging of the back face, which is an important consideration for personal protection applications such as the helmet. It has been shown earlier that the response of UHMWPE composite is significantly influenced by its architecture. Therefore, a robust model for the ballistic response of UHMWPE is desirable to optimize the protective structure and to understand load transfer to underlying structures. A numerical model to evaluate ballistic response of the Advanced Combat Helmet, also known as the ACH, has been reported in the literature.[1] However, such models do not exist for the recently developed Enhanced Combat Helmet, also known as the ECH,[2] which is the primary focus of this study. Such computer models are necessary to understand the load transfer to the head and consequent assessment of injury resulting from a ballistic event.

The composite material models used for the helmet are typically simplified for computational efficiency since inclusion of the detailed layup and fiber orientation is a challenging task even for high-performance parallel computers. Therefore, simplified homogenized or orthotropic continuum models with reduced accuracy are often employed.[3] With advancements in multiscale models, the validity for these approaches remains to be established. Similarly, the constitutive behaviors are typically obtained from experiments in 1-D or simpler configurations. Behavior of composites subjected to 2-D loading, such as bidirectional stretch, would be more appropriate for ballistic models. However, testing under such conditions to map out orientation effects at varying strain rates is cost prohibitive. Therefore, extrapolations need to be made based on limited measurements. The intention of the present study is not to develop a material model for UHMWPE material from fundamental principles, especially since accurate material test data are not available yet. Rather, the goal of this study is to develop a modeling strategy so that the mechanics of penetration and the back-face deformation (BFD) profile of helmets can be reasonably represented. These 2 characteristics determine the load transfer to the head and the brain, for which an optimal protection strategy is being sought. Therefore, our modeling strategy was to develop a computational model for UHMWPE to best fit the ballistic data, which included ballistic limit, BFD profile, and the damage sustained by the laminated structure.

The initial focus of the ballistic experiments is the flat plate geometry with cross-ply arrangement [0/90] of UHMWPE. Once a calibrated model is available for

simulating ballistic experiments with a cross-ply flat plate, the effect of the hybrid plate[4] and plate curvature in the helmet would be incorporated by carrying out additional ballistic experiments and associated modeling. While numerous ballistic data for UHMWPE exist with realistic bullets, for modeling purposes, experimental data with nondeforming projectiles are imperative to isolate composite behavior. For example, a 9-mm 124-gr full metal jacket—a commonly used bullet— deforms and fractures easily in the ballistic experiments. Modeling these experiments will introduce additional unknowns and uncertainties associated with the projectile material model and parameters. To focus on calibrating the composite model alone, fragment-simulating projectiles (FSPs) and nondeforming stainless steel sphere projectiles were used to produce V_{50} and BFD profile data, respectively.

A series of ballistic impact experiments, where various parameters of interest such as ballistic limit V_{50} and BFD were measured, were reported earlier by Zhang et al.[4] Digital image correlation (DIC) and X-ray imaging were used in those experiments to characterize time evolution of deformation, delamination, and damage of the composite. Ballistic limit velocities were also established for different thicknesses of the composite. In this report, we use those experimental measurements to develop a model for a UHMWPE composite applicable for ballistic loading conditions. A finite element (FE) model was constructed and a parametric study was carried out to identify the critical material parameters. Optimal values of these material parameters were found that best matched the test data reported in Zhang et al.[4]

The organization of this work is as follows. In Section 2, the numerical modeling of the composite laminate is presented, which includes a summary of the ballistic experiments, a description of the FE models for the projectile and panel, the material model, and the methods used to model delamination. The strategy to characterize the material parameters is discussed in Section 3. The FE models for the ballistic impact experiments were evaluated, and parametric analyses are discussed in detail in Section 4. From the parametric study, critical material properties were identified that could improve protection design. A set of material parameters was selected based on the parametric study to best match the ballistic data. Model calculations with this set of parameters are compared with the experimental results in Section 5. Main conclusions are discussed in Section 6.

2. Numerical Model of Composite Laminate

The ballistic experiments to measure ballistic limit velocity, V_{50}, and BFD experiments to measure time dependent deformation of flat UHMWPE panels and their failure characteristics were reported earlier[4] in detail. The effects of fiber

orientations, boundary conditions were studied in those experiments. A summary of the experiments used to develop the model in LS-DYNA is briefly described in the following paragraphs.

Two different sets of experiments were carried out to investigate the ballistic response of UHMWPE panels. In the first set of experiments, the ballistic limit velocity, V_{50}, of flat Dyneema panels for 17-gr (1.1-g), 0.22-cal. FSP was determined. The Dyneema HB80 panels used in the V_{50} tests were 0.45 × 0.45 m in size. The panels were clamped to a steel frame at 4 corners. The panels of 3 thicknesses with areal densities of 7.8, 8.8, and 10.7 kg/m^2, respectively, were tested.

BFD characteristics were measured in the second set of experiments, where 12.7-mm spherical steel projectiles impacted the flat UHMWPE panels at a velocity insufficient to perforate the panel. Three boundary conditions—corners clamped, edges clamped, and free—were used for the tested panels in the experiments to understand the effects of boundary constraint. DIC was used to characterize the deformation and velocity behavior of the rear of the panels during the testing. A computed tomography (CT) scan was conducted on the panels to obtain the thickness of postimpact intact material and the interior delamination failures.

All of the panels used in the BFD experiments were 0.30 m (12 inches) × 0.30 m (12 inches) × 7.8 mm (0.3 inch) thick, and their areal densities were 7.8 kg/m^2. Table 1 shows the boundary condition, impact speed, and peak BFD for cross-ply panels. The other test results are described in Section 5 where they are compared with the numerical results.

Table 1   BFD tests for cross-ply HB80 panels

Test/panel no.	Boundary condition	Projectile impact speed (m/s)	Peak BFD (mm)
458A-1	Corners clamped	440.6	28.7
458A-2	Corners clamped	424.1	27.3
546A	Edges clamped	294.1	16.1
545A	Free	292.6	16.3

We developed an FE model to simulate these ballistic experiments (both V_{50} and BFD experiments) using LS-DYNA software.[5] The focus was on cross-ply (nonhybrid) Dyneema panels to understand the impact and failure processes involved. The numerical model is capable of capturing the composite failure including interlaminar delamination. Since accurate material parameters are not available for Dyneema, we conducted a parametric study to find the most sensitive parameters. From the parametric analysis, one set of material parameters was

determined to best match the ballistic test data for the cross-ply panels. To further calibrate this model, we plan to conduct additional studies on hybrid architecture and curvature effects in the future.

2.1 Finite Element Model

The FSP, spherical projectile, and the cross-ply laminates are all symmetric along 2 fiber directions. Therefore, taking advantage of the symmetry, only one-quarter of the geometry needs to be modeled with symmetry boundary conditions. One calculation was conducted later to compare the results of full and quarter symmetry models. We found that the quarter symmetry model showed almost identical results as the full model, which provided confidence in the quarter symmetry model. The quarter symmetry model was used thereafter for calculations except where specified otherwise. Certain simplifications were made to the projectile geometry for computational convenience. The friction coefficient between Dyneema yarn to yarn is reported to be 0.05–0.07.[6] This friction value was considered to be small and was not included in the calculations.

2.1.1 Projectile

The 0.22-cal. FSP[7] was used in the V_{50} experiments. The FSP was made of 440C steel and did not deform much in the ballistic experiments as ascertained from the high-speed images. Typically, only the front edges were observed to be slightly blunted. Since the projectile is much stronger than the panel, small geometric features are not expected to play a big role in the penetration process; hence, the geometry was simplified as shown in Fig. 1a (only quarter symmetry model is shown). Specifically, the back end shape was simplified into a cylinder. The FSP was discretized with hexahedral elements. The total numbers of nodes and elements were 13,132 and 11,491, respectively.

(a)   (b)
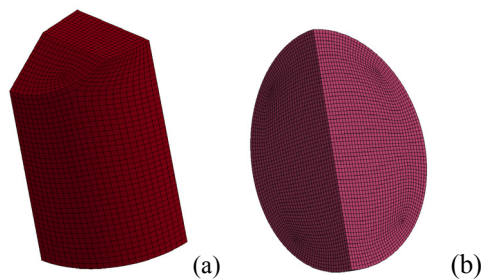
Fig. 1   FE model of a) 0.22 FSP and b) sphere projectile

The FSP material density is 7,650 kg/m^3. The yield stress for 440C steel was assumed to be 2 GPa in our model. The Young's modulus and tangent modulus were taken to be 200 GPa and 2.2 GPa, respectively.

The 12.7-mm-diameter (0.5 inch) spherical projectile used in the BFD experiment was made of stainless steel. The quarter symmetry FE model is shown in Fig. 1b. The steel ball did not show any observable deformations after the impact event. The material properties for the spherical projectile were identical to those used for the FSP.

2.1.2 Composite Panel

The panels were 0.45 × 0.45 m for the V_{50} experiments and 0.30 × 0.30 m for the BFD experiments. The difference in size is not expected to influence the ballistic limit velocity since at high-impact speeds the deformation and failure are likely to be localized. Therefore, 0.30 × 0.30 m panel sizes were used for both V_{50} and BFD calculations.

In the first series of experiments, the panels were clamped to the frame at 4 corners. No motion of the composite panel was observed at the corners before the BFD reached the peak value in the experiment. Therefore, the frame was not modeled, and panel corners were fixed in the computation. To validate this approximation, we carried out one extra simulation where the frame was included; however, only a minor difference was observed in the ballistic performance. The details are provided in Section 4.1. In the second series of experiments, free boundary condition was applied to the panels.

Three-dimensional hexahedral elements were selected to model the Dyneema panel for improved computational accuracy compared to tetrahedral elements. There are 55 plies of cross-ply UHMWPE sheets in the panels of 7.8 kg/m^2 areal density. The thickness of each ply, comprising 4 layers of [0/90]$_2$ fibers, is about 0.14 mm.

If each ply were modeled with uniform 0.3-mm mesh, a quarter million elements would be needed for just one layer in quarter symmetry. For a plate comprising 55 plies, modeling each layer entails a total element number of 14 million, which is computationally very expensive. However, large deformation was observed to occur only near the impact zone from the DIC data. The deformation amplitude was also observed to reduce as one moves farther away from the impact region, at least until the projectile perforated or stopped in the panel. Therefore, we used a nonuniform mesh—very fine mesh (~0.3 mm)—near the impact region and coarse mesh (up to 15 mm) elsewhere, as shown in Fig. 2b. The total number of nodes and elements are 5,773 and 5,636 for one layer. Fiber breakages were expected to occur only in the impact zone. As shown in Fig. 2a, the panel was divided into impact

zone and nonimpact zone. Therefore, contact with erosions was used only for the impact zone for improved computational efficiency.

If the panel having an areal density of 7.8 kg/m^2 were modeled with 55 layers, large computational resources would be needed because of the necessity to model contact between each adjacent layer. Therefore, we chose to use a reduced number of "fused" layers in the computational model, keeping the panel thickness the same. The effect of using different number of fused layers was studied in Section 4.1, and it was found that the model with reduced number of fused layers gave reasonable results and was much more efficient. The sample FE model for the spherical projectile and panels (20 fused layers were used) is shown in Fig. 2a. Each layer is shown in a different color for clarity.

(a)   (b)
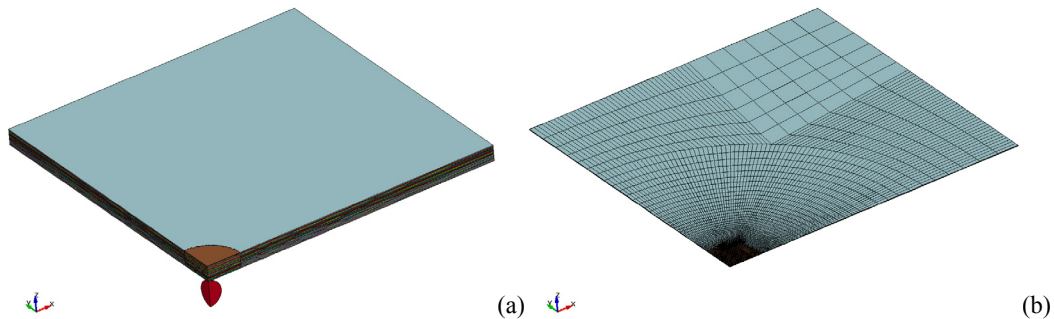
Fig. 2   FE model for a) projectile and panel and b) one ply

2.2 Material Model

The CT scan of the panels after impact[4] showed that the composite failed through tensile breakage, shear failure, crushing, and delamination. In addition, UHMWPE has been shown to exhibit damage softening[8] and strain rate effect[9] in the stress-strain curve. We chose a material model (Mat 162) in LS-DYNA[5] that could model such behavior and used the tie-break contact method to model delamination explicitly. Some of the failure modes available in this material model were switched off to avoid premature failure due to fiber compression, matrix shear, and delamination (which was modeled through tie-break contact separately).

A limited amount of material test data is available in the literature for Dyneema laminates. Because of clamping issues arising out of the low friction coefficient for Dyneema, the measured tensile strength is greatly dependent on the sample thicknesses.[10] Dynamic tensile tests[11] show strong strain rate effects for Spectra Shield LCR material (which is a similar material to Dyneema). The strength increases significantly with strain rate, while the material becomes more brittle at a high strain rate.

The tensile strength of Dyneema laminate is reported to be around 500 MPa.[12,13] Because of low shear strength, the specimen could experience shear/pullout failure at the grips. This failure mode would result in underestimation of the tensile strength. Recently, tensile tests have been conducted on HB26 (HB26 and HB80 are both made of SK76 yarns) for [0/90] laminate[9] with dog-bone specimens to minimize gripping issues. The tensile strength was found to increase to about 750 MPa; however, the failure strain was lower than the values reported earlier in Iannucci et al.[12] and Iannucci and Pope[13] These tests[9] were conducted at low strain rates (10^{-4} to 10^{-2}/s). Dyneema laminate has a strain-rate-dependent stress-strain curve in the low strain rate regime. In the same paper, the stress-strain curves for the Dyneema SK76 yarn for strain rate from 10^{-4} to 10^3/s is also reported. The material showed negligible strain rate dependence when the strain rate is higher than 10^{-1}/s. Based on this observation, we ignored the strain rate effect in our model since in the impact experiments the strain rate is expected to be higher than 10^{-1}/s. However, this might not be true when the projectile starts to slow down and rebounds. In this stage, the material experiences a low strain rate. Unless the strain rate effect at lower strain rates is included, the panel response after the peak BFD would not be accurate. This is not an issue since our main focus in this paper is to model the panel response up to the peak BFD. The peak BFD is the critical parameter for determining whether the helmet would impact the skull after a threat is stopped. Russell et al.[9] pointed out that the yarn strength is underestimated because of the stress concentration, abrasion of the yarn surface, and waviness within the yarn. The strength was reported to be 3.8 GPa both in Russel et al.[9] and Chocron et al.,[14] which was selected as the strength of Dyneema SK76 yarn in this work. For the [0/90] laminates, considering that only fibers in the 0° or 90° direction are subjected to the loads and the volume ratio of matrix is 20%, the strength for the laminates equals 3.8 GPa*(1–0.2)*0.5 = 1.5 GPa using the rule of mixture assuming that the matrix does not contribute to the laminate strength. The Young's modulus for SK76 is reported to be 132 GPa,[14] whereas the Young's modulus for the laminate is 52.8 GPa.

The tensile stress-strain curve for the [45/–45] Dyneema laminate is reported in Russel et al.[9] and Nazarian and Zok[15] The curve represents the in-plane shear response of [0/90] laminates, which is a combination of matrix shear modulus and friction between fibers along 0° and 90° directions. The response is very sensitive to the strain rate, at least in the range of 10^{-4} to 10^{-2}/s. The shear modulus increases as the strain and the strain rate increase. No high-rate data are reported. Assuming a similar high-rate response as tensile experiments, we ignored the strain rate effects in this study. The modulus from the stress-strain curve was found to be in the range of 50–90 MPa for various strain rates, which was 2 to 3 orders of magnitude lower than the tensile modulus of 52.8 GPa for the laminate. Since Dyneema HB80 is also

made of SK76 yarns, similar properties are expected. Since no test data are available at high strain rates, the shear modulus, G_{ab}, was also evaluated in the numerical model using the experimental data.

Each ply of the panel was made of $[0/90]_2$ layers of unidirectional laminates sheets. To be more efficient, 4 layers of $[0/90]_2$ cross-ply were modeled as one orthotropic layer as opposed to 4 individual layers (a 0° layer, a 90° layer, a 0° layer and a 90° layer). It was shown in Heisserer[10] that the properties along 0° and 90° are not the same. However, as shown in Fig. 3, the BFD contour from the DIC test data exhibited a diamond shape. Two red squares were drawn on the plot to indicate that the length and width are almost the same for the contour levels, (i.e., the response is symmetric about 0° and 90° directions). This implies that the properties are similar in 0° and 90° directions in the panels. Thus, identical properties were used for the 2 fiber directions in this work.
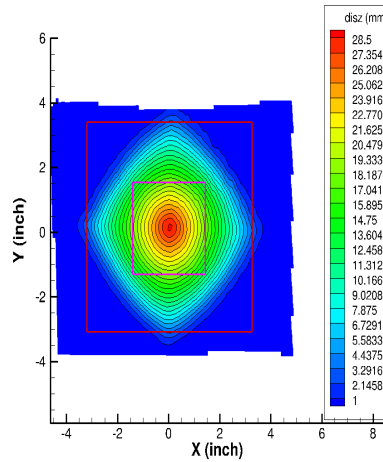
Fig. 3   Sample BFD contour for test 458A-1

2.3 Delamination Model in the Composite Laminate

Delamination is a very common failure mode in composite laminates. Modeling delamination is still a challenging task. In Faux et al.,[3] a progressive damage model was developed in ALE3D to simulate the high-speed penetration in Dyneema panels. ALE3D uses an arbitrary Lagrangian-Eulerian framework. The delamination can be captured with an internally stored crack strain. ParaDyn, a Lagrangian code, was also used for simulation in Faux et al.,[3] in which the composite was modeled with orthotropic [0/90] sliding layers (one element along thickness direction per layer) with automatic contact (SAND) defined. Delamination can be simulated in LS-DYNA by failing the elements, by using a

tied-contact-with-failure option between adjacent layers, or by using cohesive elements. In this work, the tied-contact option was used between adjacent layers to model the delamination.

2.3.1 Matrix Failure

The material fails in the model when the matrix material exceeds the prescribed strength in the direction parallel to the laminates. Upon failure, the load-carrying capability in the thickness direction (including the 2 shear stresses and normal tensile stress) is reduced, and the compressive load can be supported in the thickness direction. By tracking the history variables, we could plot the delaminated area.

This method is very efficient for calculations. However, delamination is not actually modeled since there is no gap generated upon delamination unless the failed elements are eroded.

2.3.2 Tied Contact

The second method employed to model the delamination in the composite material was by defining tied contacts between adjacent layers. Initially the layers are tied together. The tied contact fails when the following failure criterion is satisfied:

$$\left(\frac{\sigma_n}{S_n}\right)^2 + \left(\frac{\sigma_s}{S_s}\right)^2 \geq 1, \tag{1}$$

where S_n is normal failure strength, S_s is shear failure strength, and σ_n and σ_s are tensile and shear stress, respectively. If the normal stress σ_n is compressive, it is set to zero (i.e., the tied contact can only fail under normal tensile stress or shear stress). After the tied contact fails, the contact between adjacent layers is changed to regular surface-to-surface contact. However, in high-speed penetration problems, the material would fail and erode, and the regular contact algorithm cannot update the contact surfaces automatically. Therefore, the eroding contact option was also defined around the impact zone, where fiber breakage was expected. This method ensured that all of the contacts worked correctly after tied contact surfaces failed.

Material weakening is not modeled in this method. When the failure criterion as described in Eq. 1 is satisfied, the tied contact fails and the nodes on the adjacent surfaces are no longer tied together. A gap is thus generated between the layers. The 2 layers can contact again if they move toward each other. This appears to be a better way to simulate the delamination failure.

Cohesive zone model[16] can also be used to model the interface between adjacent composite layers. In our previous work,[17] cohesive elements were used to model delamination; however, more central processing unit (CPU) time was required because of the presence of additional elements and additional contact between material layers. Since the method described previously is computationally more efficient, we did not evaluate the cohesive zone model in this study.

3.   Material Parameters Characterization Strategy

The material parameters for Dyneema include the density, Young's modulus along $0°$ direction E_a, Young's modulus along $90°$ direction E_b, fiber tensile strengths, transverse Young's modulus E_c, 3 Poisson's ratios, in-plane shear modulus G_{ab}, transverse shear moduli G_{bc} and G_{ac}, interlaminar tensile strength S_n, crush strength, and the strain softening parameter A_m.

Since the cross-ply HB80 panels have identical properties along the 2 principal fiber directions, the material parameters reduce to the densities E_a ($E_b = E_a$), E_c, G_{ab}, G_{ac} ($G_{bc} = G_{ac}$); crush strength S_c; strain softening parameter A_m; Poisson's ratios ν_{ab} and ν_{ac} ($\nu_{bc} = \nu_{ac}$); the interlaminar tensile strength or the tensile failure strength of tie contact S_n. The density is available. The fiber tensile strength and fiber Young's modulus E_a were determined previously from existing test data. Poisson's ratios are small and are assumed to be zero in this report. A simulation was run with the Poisson's ratios of $\nu_{ab} = 0.0133$ and $\nu_{ac} = 0.0144$ from Levi-Sasson et al.[8] and the difference in the panel response was minor as shown in Fig. 4. Thus 6 material parameters need to be determined: 1) interlaminar tensile strength S_n, 2) in-plane shear modulus G_{ab}, 3) transverse shear modulus G_{ac}, 4) transverse Young's modulus E_c, 5) crush strength S_c, and 6) damage softening parameter A_m.
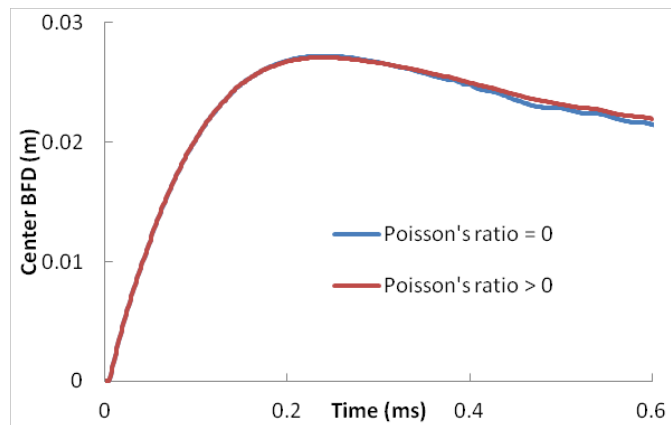

Fig. 4   Effect of Poisson's ratio

Since we did not conduct material tests for the Dyneema panels, we carried out a parametric study to find one set of material parameters to best match the experimental data. The panel response is nonlinear and dependent on the material parameters. There are 6 unknown material parameters; hence, at least 6 sets of test data are required to find one set of parameters to match the test data. This set of parameters may not be unique, but they can at least match the test data within the test conditions of the V_{50} tests and BFD tests conducted in this work.

The modeling focus in this work was on the nonhybrid HB80 panels. Therefore, only the test data from 458A-1, 458A-2, and 545A panels (panel 546A was excluded because of similar results to panel 545A and not well-defined boundary conditions for the numerical model), were used along with the V_{50} test data for 3 different thickness cross-ply panels, resulting in a total of 6 tests.

Figure 5 shows the variables from the experiments that were compared with the numerical results. The first is the time history of center BFD, which is the maximum deflection in the back face. The second is the deformation zone size in the symmetry plane passing the impact location for the back face. The center BFD and deformation zone size together give the section profile for the symmetry plane. The third is the time history of BFD contour, from which the BFD shape can be determined. The first 3 can be obtained from the DIC data. The fourth is the remaining thickness of intact composite. The fifth is the final delamination failures (including fiber breakage). The last 2 variables could be obtained from CT scan of posttest panels.

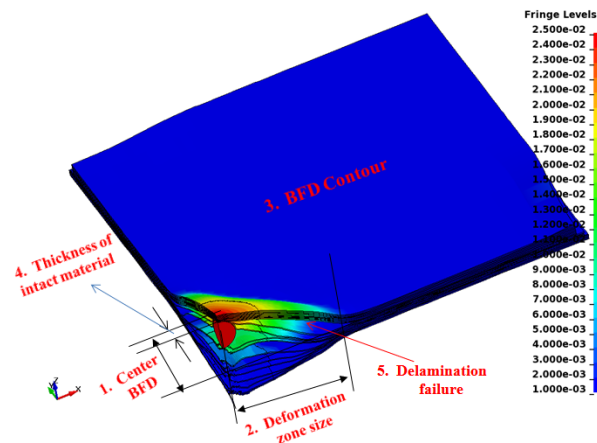**Fig. 5   Variables to be compared between model and experiments**

The 6 tests and available test data are listed in Table 2. The first 3 tests are similar, and only one test is needed to characterize the material model. Similarly, only one test is needed from test d and test e (the impacting velocity was slightly different). The selected 6 sets of test data for model comparison are italicized in the table. Of

course, more test data can be used for model characterization. After the model parameters were calibrated, we validated the model with the remaining test data (data in normal font).

Table 2   Test data selection for model characterizations

Data set	Test description	Test data
a	V_{50} test of cross-ply (7.8 kg/m^2)	*1. Normalized V_{50} (1.00)*
b	V_{50} test of cross-ply (8.8 kg/m^2)	Normalized V_{50} (1.09)
c	V_{50} test of cross-ply (10.7 kg/m^2)	Normalized V_{50} (1.26)
d	BFD test of panel 458A-1 (440.6 m/s)	*2. Peak center BFD (28.7 mm)* *3. Percentage of thickness of intact composite (40.3%)* *4. Deformation zone size*
e	BFD test of panel 458A-2 (424.1 m/s)	Peak center BFD (27.3 mm) Percentage of thickness of intact composite (50.4%) Section profile of back face
f	BFD test of panel 545A (292.6 m/s)	*5. Peak center BFD (16.3 mm)* *6. Percentage of thickness of intact composite (76.4%)* Deformation zone size

Note: The selected 6 sets of test data for model comparison are italicized.

4.   Model Parameters

The numerical model described previously was used to simulate the responses in the nonhybrid HB80 panels under impact loading conditions. A parametric study was conducted to identify critical material parameters.

Each ply, which includes 4 layers with [0/90]$_2$ fiber orientations, have identical properties along the 0° and 90° directions; therefore, the fabric model could be used with longitudinal properties assigned to both the 0° and 90° directions. This approximation is computationally efficient but less accurate than modeling each layer separately and defining tie-contact between them.

In the first setup numerical model, the panel was modeled with 20 fused layers; one element per layer along the thickness direction and a quarter model with symmetry boundary conditions; the steel frame was not modeled for panel 458A-1. This model was used for debugging purpose and for rough comparison with test data. The calculations were carried out on the Department of Defense High-Performance Computer Pershing cluster, which has 16 cores on each node. LS-DYNA Version 7.0.0 (double precision serial/SMP) was used for the calculations.

4.1 Model Evaluation

For a computationally efficient model, several simplifications were explored (e.g., use of quarter symmetry, using a single orthotropic layer to represent multiple laminates, removing the frame in the calculation, and minimum mesh resolution in the thickness direction to model bending effects).

4.1.1 Full Model vs. Quarter Symmetry Model

One calculation was performed to determine the validity of using a quarter symmetry model with symmetry boundary conditions to represent the full model. Figure 6 shows the time history of BFD for both models. The BFD is almost identical until the peak (the peak BFD has 0.8% difference). Many elements failed and eroded in the calculations, which caused only a minor difference between models. However, the quarter symmetry model ran much faster (3.3 h for quarter symmetry model vs. 20 h for full model). Therefore, the quarter symmetry model was used subsequently.
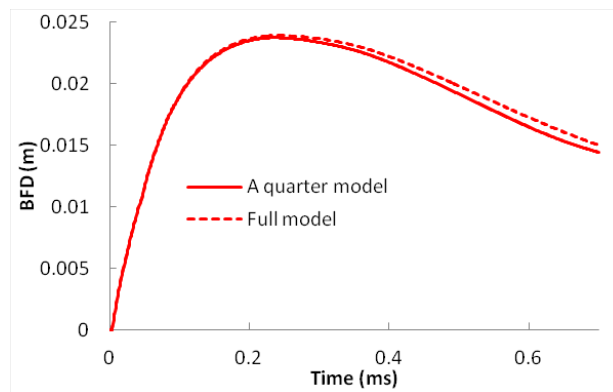
Fig. 6   Comparisons between full model and one-quarter model

4.1.2 Number of Elements per Layer

To include the effect of bending, more than one element per layer along the thickness direction is necessary. Four cases were run: 1, 2, 3, and 4 elements per layer were used along the thickness direction. Figure 7 shows the time history of BFD for these 4 cases. The BFDs are smaller when the bending effect is accounted for. However, the BFDs have reasonable agreements when 2–4 elements per layer were used along the thickness direction.
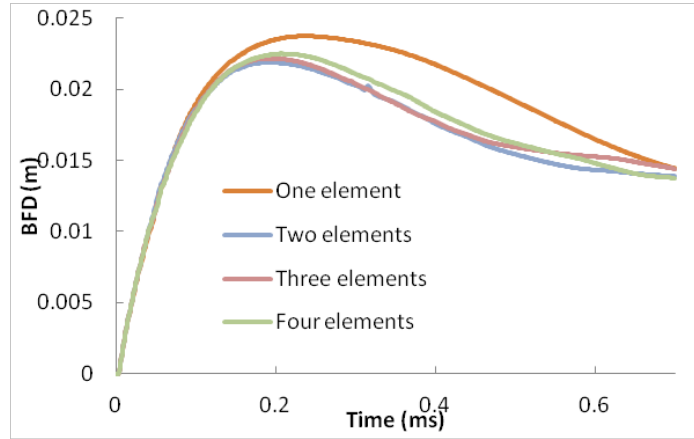
Fig. 7   Effect of the number of elements per layer

Figure 8 shows the deformations at 0.3 and 0.7 ms when different numbers of elements were used per layer. When more than one element was used per layer, the gap was larger between adjacent layers after delamination occurred. Another difference is the section profile of the back face, as shown in Fig. 9. The profiles are similar when the number of elements per layer is 2 and higher. The CPU time ratio is 1.0:2.0:4.9:6.4 for the cases of 1, 2, 3, and 4 elements per layer. One good choice is to use 2 elements per layer, which can both capture the profile but still be efficient. Two elements per layer were used in the remaining calculations.

0.3 ms   0.7 ms
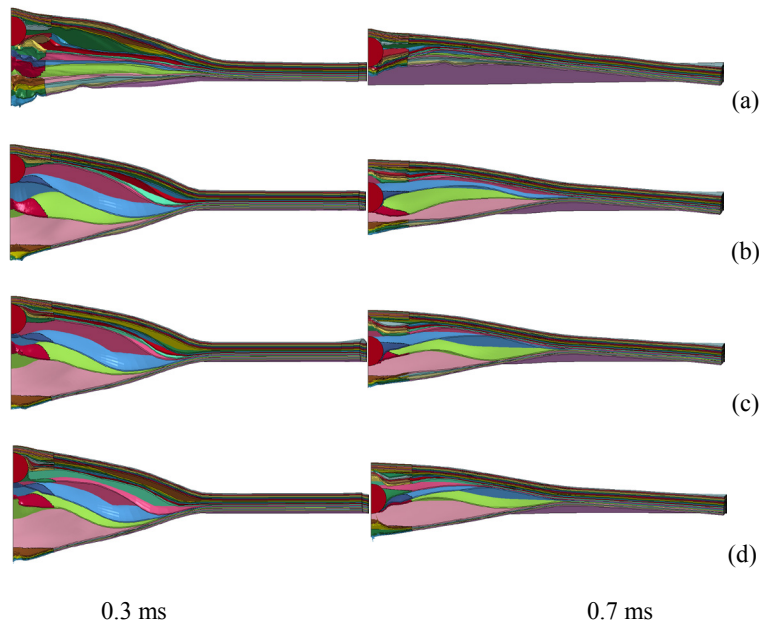
Fig. 8   Deformations at 0.3 ms (left) and 0.7 ms (right) for a) 1, b) 2, c) 3, and d) 4 elements per layer

14
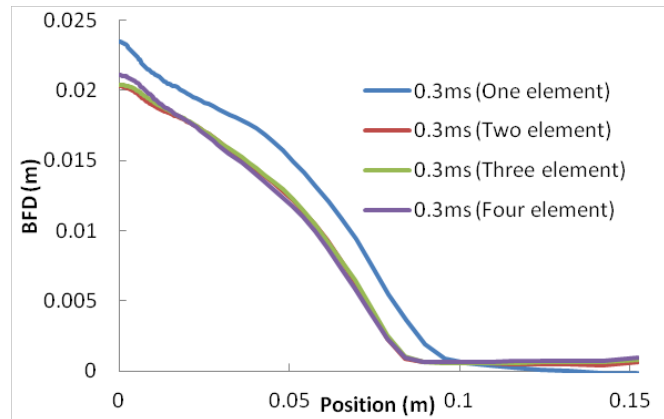
Fig. 9   Penetration section profiles at 0.3 ms for different numbers of elements per layer

4.1.3   Effect of Frame

The frame used to clamp the Dyneema panels at the 4 corners was modeled to explore the effect of boundary conditions. Figure 10b shows the FE model (one-quarter model was used with symmetry boundary conditions; the meshes of panel and projectile were not shown). The actual dimensions of the steel frame from the experiments were used. A rigid material was assumed and the short side of the frame was not modeled, which was not in contact with the panels, as shown in Fig. 10a. Contacts were defined between the panel back face and the frame. The panel was still fixed at the corners to represent the clamps. The frame thus behaves like a rigid wall to prevent the panel from deflecting (the panel can still slide on the frame).
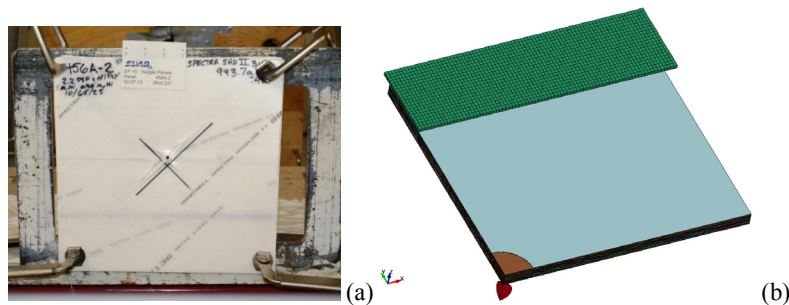
Fig. 10   a) Test setup (front view) and b) FE model with steel frame (one-quarter model, back view)

The effect of the frame turns out to be very small, as shown in Fig. 11. The frame only has effect for later response after the peak BFD. This validates our approach of using a free-boundary condition in place of the frame in the model.
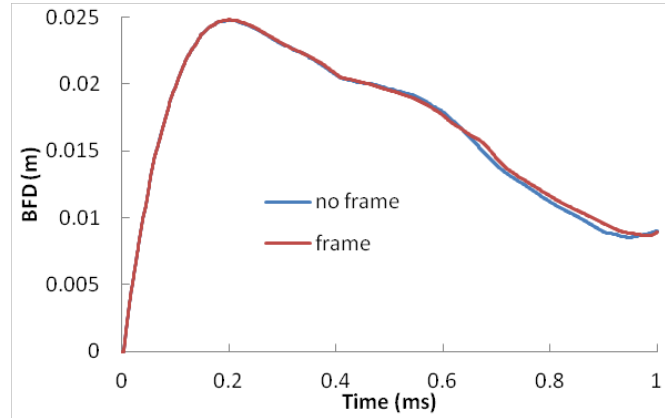
Fig. 11   Effect of frame on the BFD time history

4.1.4 Number of Layers

There are 55 plies in the panel of 7.8 kg/m^2 areal density and each ply includes 4 layers of [0/90]$_2$ fiber. If [0/90] layers are modeled as one layer of orthotropic material, 110 layers would be needed for the panel. This would require large computational resources because of the necessity to model contact between the layers. We tried modeling the panels into 5, 10, 15, 20, 25, 30, 40, and 50 fused layers, keeping the panel thickness the same.

Figure 12 shows the time history of BFD for different fused layers. The increasing slope is almost identical except when the number of layers is 5. The rebounding phase is similar when the number of layers is 20 and above. Figure 13 shows the penetration profiles at 0.2 ms for all these cases. The results are similar when 15 and more layers were used in the model. At least 15 layers are necessary to capture the delamination.
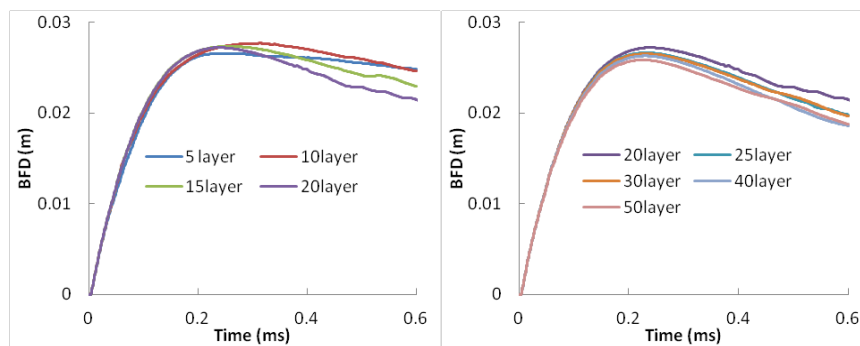
Fig. 12   Effect of number of "fused" layers on the BFD time history

16
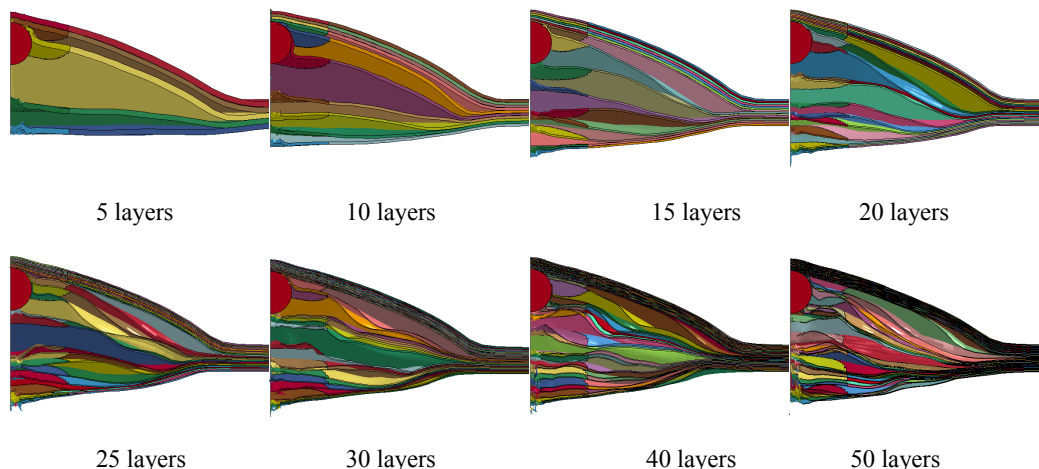
Fig. 13 Deformations at 0.2 ms for different numbers of fused layers

Table 3 compares the peak BFD, percentage of intact composite thickness, and CPU hours for the cases of different numbers of layers. Twenty fused layers (the mesh aspect ratio is 1.5) were selected because of affordable CPU time.

Table 3 Comparison of peak BFD, remaining thickness, and CPU hours for different number of layers used to model the panel

Number of fused layers	Mesh aspect ratio	Peak BFD (mm)	Peak BFD (50 layers as base) (%)	Remaining thickness (%)	CPU (h)
5	2.6	26.6	2.9	40	1.3
10	1.3	27.7	7.1	40	4.1
15	1.1	27.4	5.9	47	9.3
20	1.5	27.2	5.3	45	11.0
25	1.9	26.6	3.1	44	14.9
30	2.3	26.5	2.7	43	25.3
40	3.1	26.3	1.8	45	34.3
50	3.8	25.8	0.0	46	55.8

The numerical model used for the parametric study was finalized: a quarter symmetry model excluding the frame with 20 fused layers and 2 elements per layer along the thickness direction.

As discussed previously, not all parameters for Dyneema HB80 are available. The parameters that needed to be calibrated through the parametric study were 1) interlaminar tensile strength S_n, 2) in-plane shear modulus G_{ab}, 3) transverse shear modulus G_{ac}, 4) transverse Young's modulus E_c, 5) crush strength S_c, and 6) damage softening parameter A_m.

A parametric study was conducted to determine the sensitivity of these parameters. The most sensitive parameters need to be studied more carefully or obtained

experimentally. From the sensitivity analysis, a set of parameters was determined based on the comparison with test data. The tests used for parametric study comparison are the V_{50} test of cross-ply (7.8 kg/m^2 areal density) and the BFD tests (test 458A-1 and 545A).

4.2 Parametric Study

The fiber Young's modulus and strength (σ_a, σ_b) are based on previous analyses from test data in Russell et al.[9] The available parameters for the base calculation are as follows: Density = 990 Kg/m^3, $E_a = E_b = 52.8$ GPa, $\sigma_a = \sigma_b = 1.5$ GPa, $\nu_{ba} = \nu_{ca} = \nu_{cb} = 0$, and failure strain = 3%.

The base parameters for the 6 unknown parameters were normalized to be 1. In the parametric study, the material parameters are all normalized.

4.2.1 V_{50} Experiments

A parametric study was conducted for the 6 unknown parameters. The V_{50} test of HB80 cross-ply (7.8 kg/m^2 areal density) was used for this parametric study. The projectile impact speed used in the calculation equaled the V_{50}, which has normalized value of 1.

Figure 14 shows the sample penetration processes for both perforation (the projectile perforated the panel) and nonperforation cases (the projectile was stopped by the panel). Initially, the composite in front of the projectile failed. Delamination failures occur in this stage. A great amount of projectile kinetic energy is transferred to the composite. Around 50 μs, the fibers start to have many stretches in the panel back layers. If the projectile still has enough energy to penetrate the panel, the composites fail because of fiber breakages (at 100 μs, the panel already has a through hole); otherwise the projectile will either be arrested in the panel or rebound.

<div align="right">5 μs</div>

<div align="right">10 μs</div>

<div align="right">20 μs</div>

<div align="right">50 μs</div>

<div align="right">100 μs</div>

<div align="right">150 μs</div>

(a) Nonperforation   (b) perforation
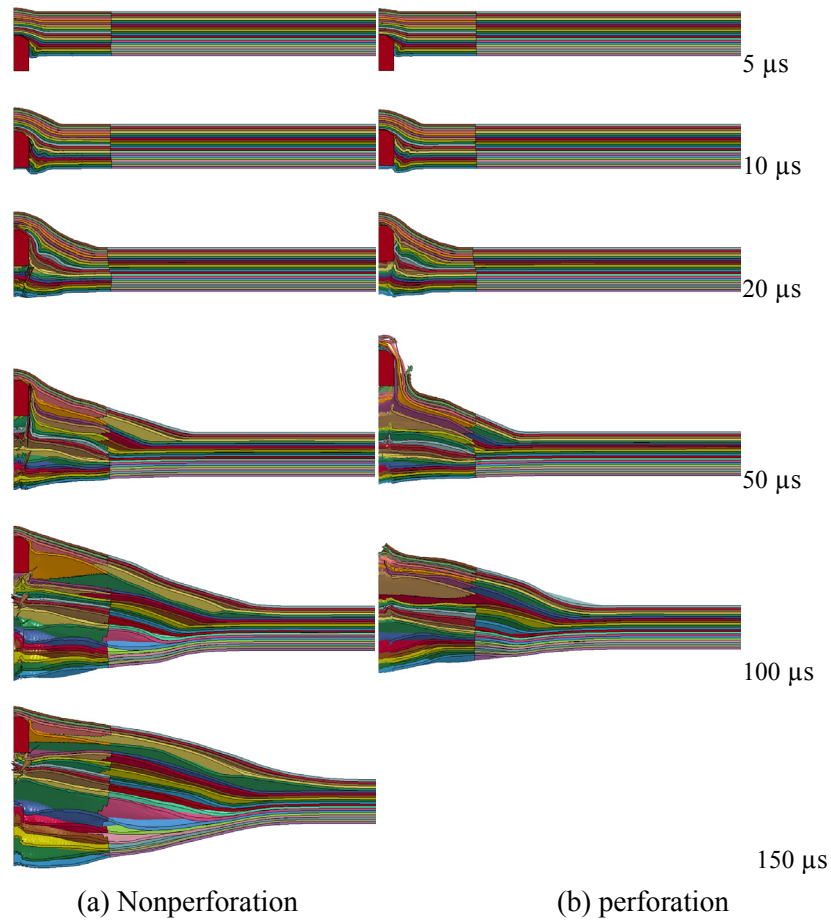
Fig. 14   Sample penetration processes for a) nonperforation and b) perforation of the panels

Figure 15 shows the time history of the projectile kinetic energy for different values of crush strength and the damage softening parameter; other parameters were also evaluated in the study but are not shown in the figure. The following observations can be made:

- The energy drop rate is only dependent on the crush strength S_c and the damage softening parameter A_m.

- The energy drop can be divided into 2 stages. The first stage is when the materials in front of the projectile deform and fail, which can absorb a lot of the energy. Fast energy drop occurs for this stage. The second stage is the further fiber stretches in the back layers, which can absorb additional energy. The second stage is mainly for the case when the projectile is stopped by the panel. The 2 stages have already been discussed in Fig. 14. The energy absorption in the second stage cannot be neglected and can be 10%–20% of the total energy absorbed.
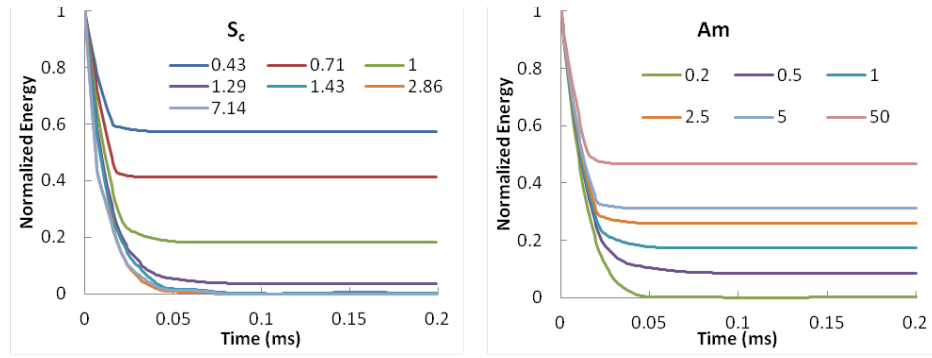
Fig. 15 **Time history of projectile kinetic energy for different values of parameters S_c and A_m**

The percentage of projectile kinetic energy absorbed in the panel is plotted in Fig. 16 for different material parameters. The following conclusions can be drawn:

- The tensile strength of the tied contact S_n has minor effects on the total kinetic energy absorbed.

- As the in-plane shear modulus G_{ab} increases, the projectile remaining energy increases.

- The percentage of absorbed kinetic energy decreases as the transverse shear modulus G_{ac} increases; however, it levels off for large shear modulus values.

- As the transverse Young's modulus E_c increases, the composite becomes stronger and can absorb more kinetic energy. However as E_c further increases, the composite becomes more likely to fail because of crush failure (the transverse compressive stress is proportional to the transverse Young's modulus E_c), resulting in absorption of less kinetic energy.

- Less material would fail because of crush failure and the composite would absorb more kinetic energy when the crush strength Sc increases. When the crush strength reaches a critical value, the material would not fail because of crush failure and the composite cannot absorb additional energy.

- As the damage softening parameter, A_m, increases, the material behaves in a more brittle fashion and can absorb less kinetic energy.

20

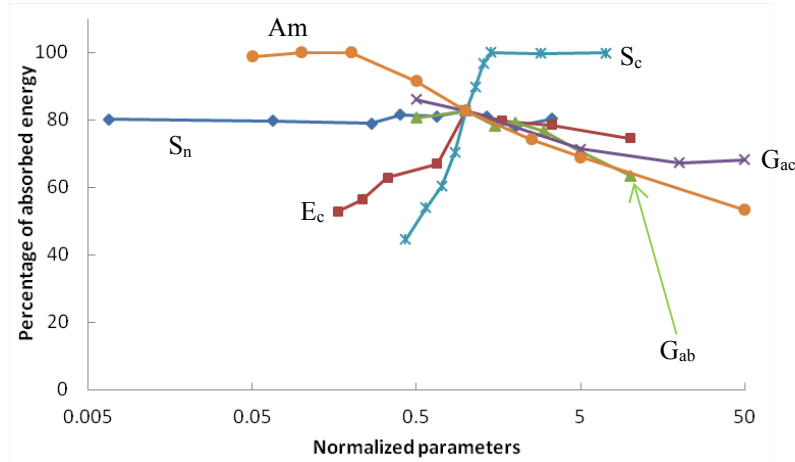**Fig. 16   Percentage of kinetic energy absorbed for different material parameters**

From the previous analysis, the slowdown of the projectile includes 2 stages. The first stage is due to the fiber breakage and crush failure in the composite. The second stage is due to the fiber stretching in the rear undamaged layers. The energy lost during the second stage cannot be neglected.

The energy drop rate only depends on the crush strength and damage softening. If the time history of the projectile energy can be measured in the ballistic tests, these 2 parameters can be further characterized.

The ballistic performance of the composite panels depends mainly on the transverse Young's modulus E_c, the crush strength S_c, and the damage softening parameter A_m. However only A_m and S_c can be easily adjusted so that the projectile can be stopped by the panels (100% kinetic energy is absorbed).

4.2.2   BFD Experiments

Similar parametric studies were conducted for the BFD experiments. The experiments on panel 458A-1 and panel 545A were used for this parametric study. The material properties for the base case were kept the same as the V_{50} parametric study.

Figure 17 shows the penetration processes. After impact, the material in front of the projectile fails and produces a hole in the panel. Some delamination occurs near the projectile. After about 50 μs, the composites do not fail but stretch with delamination propagations. After around 200 μs, the panel back center and projectile start to rebound.

| 10 µs | 20 µs | 30 µs | 50 µs |

| 100 µs | 200 µs |
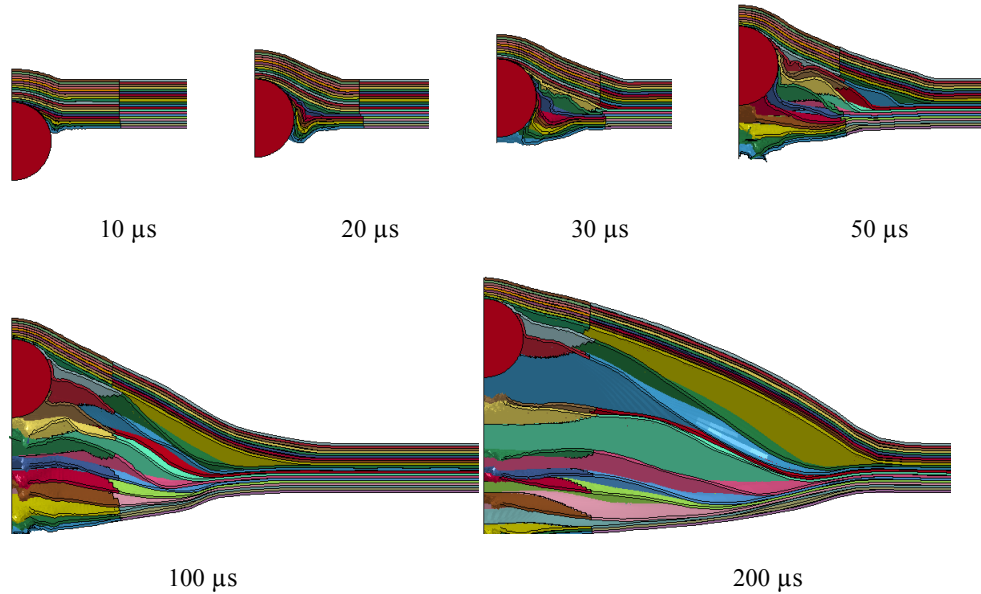
Fig. 17   Sample penetrations for BFD tests

Figure 18 shows the corresponding time history of the projectile kinetic energy and projectile speed (absolute value). The energy drop is found to be faster for stage 1 (up to 50 µs) because of quick energy transfer to the composite. A lot of composite material fails during stage 1. The second stage involves a much slower energy drop until the panels rebound (around 230 µs when the projectile speed starts to increase from 0). The energy drop in the second stage is about 20% of the total energy.

(a)   (b)
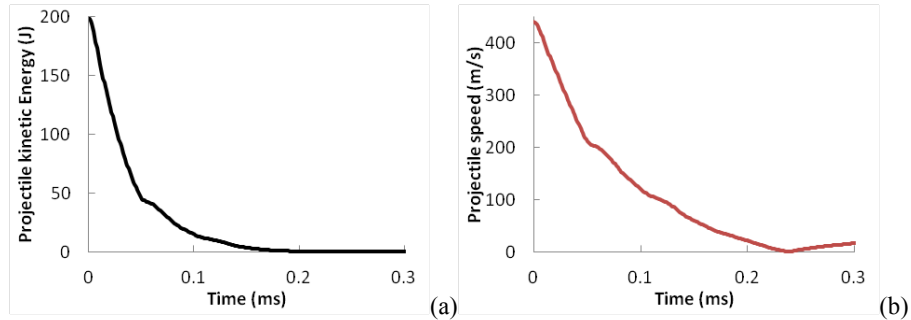
Fig. 18   Time history of projectile: a) kinetic energy and b) velocity

Figure 19 shows the time history of the center BFD for different material parameters. The time history of the center BFD can be divided into 2 stages as previous (of course, there is a third rebounding stage, but this is not our focus in this report). The center BFD increase rate in the first stage appears not to depend on the material parameters. However, the BFD increase in the second stage is largely dependent on the material parameters, when the composite in front of the projectile does not fail and continues stretching until the kinetic energy is dropped to zero before rebounding.
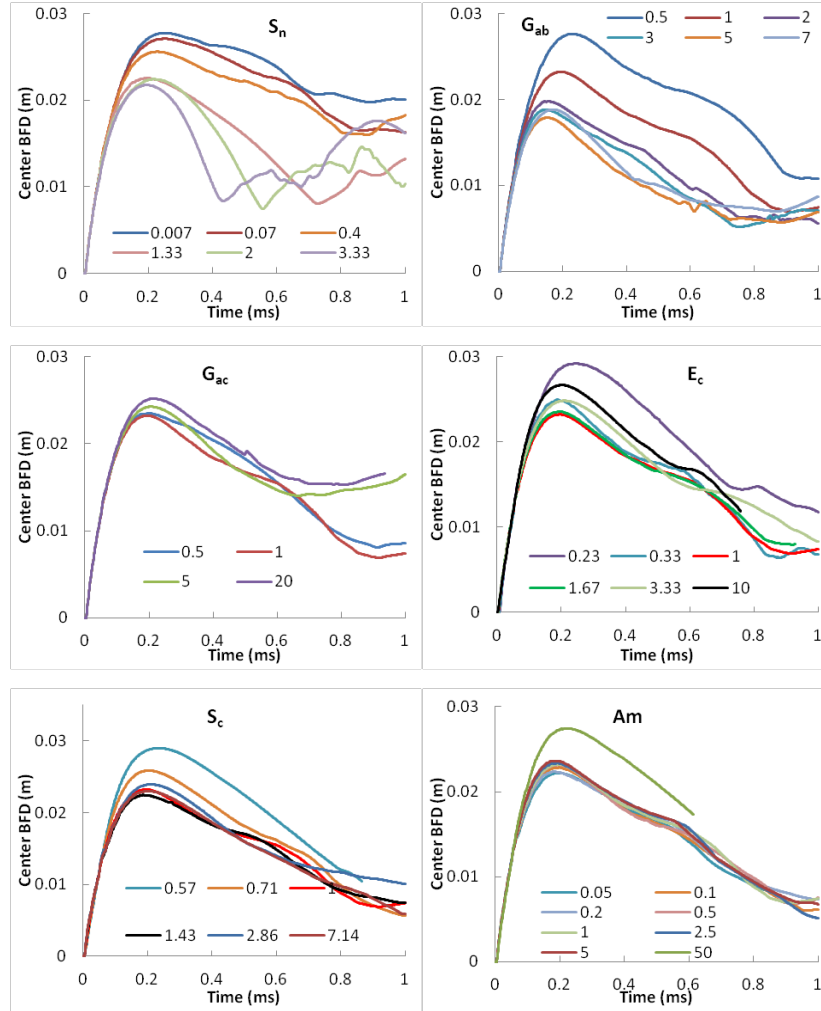
Fig. 19   Time histories of the center BFD for different material parameters

Figure 20 shows the peak center BFD and intact composite thickness normalized by test data for different material parameters.

- As the tensile strength increases, the peak center BFD drops but the intact material thickness does not change much (one fused layer failure results in 0.13 decrease in the curve). For the parameters used, the peak BFD is underpredicted for test 458A-1, while overpredicted for 545A for a wide range of tensile strengths. This is due to either incorrect values of other 5 material parameters or different failure mechanisms involved in the high-speed BFD and medium-speed BFD tests, which are not captured by current model.

- Both the peak center BFD and intact composite thickness drops with the in-plane shear modulus G_{ab}.

23

- There is a minor effect of transverse shear modulus G_{ac}.

- As the transverse Young's modulus E_c increases, the composite becomes stronger; therefore, less material fails and deflection is reduced. However, this trend changes as E_c rises above a critical value when crush failure is easier to occur for the material, which would make the final intact composite thinner and lead to a higher BFD.

- The effect of the crush strength S_c is similar to the effect of the transverse Young's modulus. The difference is that as the crush strength becomes very high, no material will fail under crush, and the BFD and intact composite thicknesses do not change.

- As the damage softening parameter A_m increases, the material becomes more brittle, more composite fails, and the peak BFD increases.

- Overall, the panel responses at high impacting speed are more sensitive to the material parameters than at medium impacting speed.

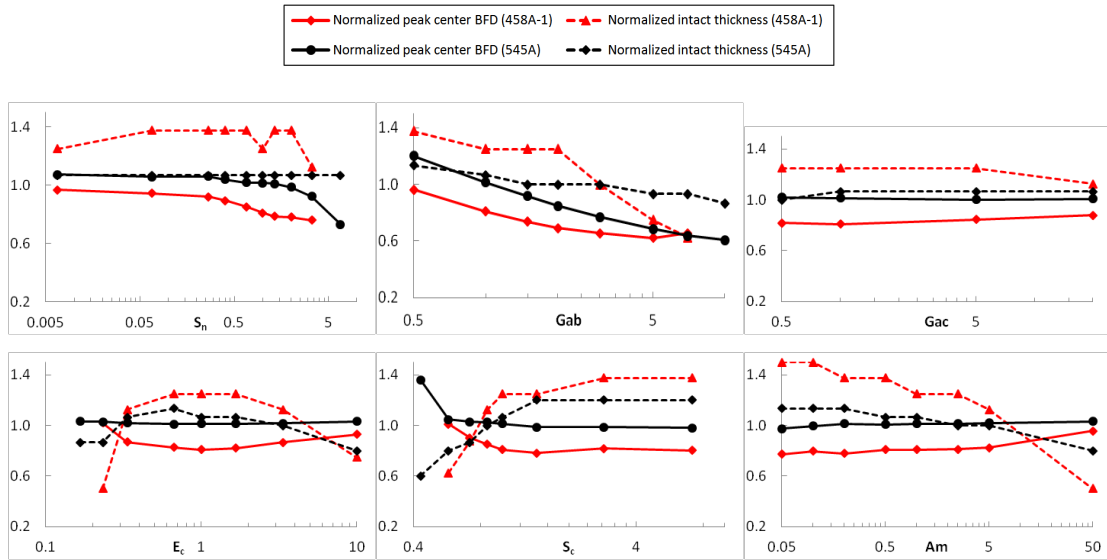**Fig. 20   Normalized peak center BFD and normalized intact composite thickness (normalized by the test data) for different material parameters**

Another test data used for model characterization is the deformation zone size at 100 μs, which is shown in Fig. 21. The most sensitive parameter is the in-plane shear modulus G_{ab}, and then the crush strength S_c and transverse Young's modulus E_c.
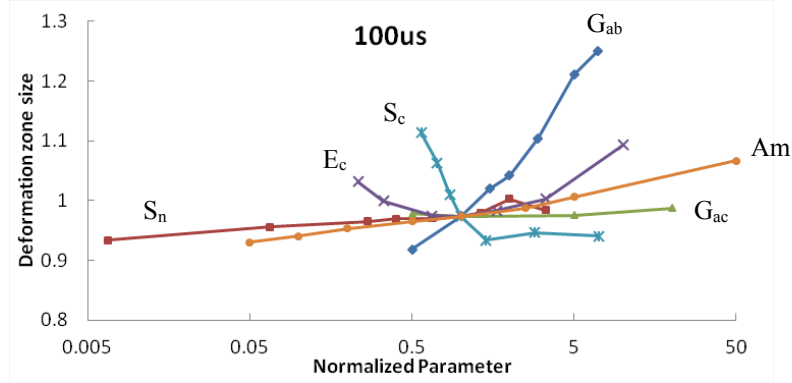
Fig. 21   Deformation zone size at 100 μs for different material parameters

The V_{50} and BFD are 2 most important ballistic characteristics for the helmet performances with higher V_{50} and lower BFD being desirable for better protection. The parametric study showed the sensitivity of critical material parameters on these ballistic characteristics as follows:

- Higher interlaminar tensile strength S_n has a minor effect on V_{50} but decreases BFD.

- Higher in-plane shear modulus G_{ab} lowers both V_{50} and BFD.

- Higher transverse shear modulus, G_{ac} lowers V_{50} but has a minor effect on BFD.

- Higher transverse Young's modulus E_c increases V_{50} but the effect is not monotonic for BFD.

- Higher crush strength S_c results in higher V_{50} and lower BFD.

- Higher damage softening parameter A_m results in lower V_{50} but higher BFD.

For improved ballistic protection, helmet material needs to have higher interlaminar tensile strength S_n, transverse Young's modulus E_c, and crush strength S_c but smaller transverse shear modulus G_{ac} and damage softening parameters A_m. For a given fiber and matrix combination, some of these material parameters (the average material parameters to be more precise) can be changed, for example, by changing the architecture. Hybrid panels[4] possess higher average in-plane shear modulus G_{ab} by using a rotated laminate architecture. Based on the parametric study, hybrid panels are expected to exhibit lower V_{50} and lower BFD as observed in experiment.[4]

4.3 Characterized Material Parameters

The parametric study was used to find one set of material parameters that can best match the test data. The effect of the transverse Young's modulus E_c is not monotonic. E_c was determined after the other 5 parameters are finalized. The steps we used to determine the material parameters are as follows:

Step 1: The tensile strength S_n has minor effects on the V_{50}, thickness of intact material, and deformation zone size but mainly affects the peak BFD. No value of S_n can be found to match the peak BFD with test data for both panel 548A-1 and 545A from Fig. 20. However, the test data for panel 458A-1 shows that the time between the peak BFD and minimum BFD is about 0.7 ms (see Section 5.2). Figure 19 shows that the tensile strength S_n is the key parameter to control this time and when S_n has a value of 0.4 it gives the closest time to 0.7 ms.

Step 2: To match the V_{50} data (100% projectile kinetic energy is absorbed) in Fig. 16, the parameter, A_m can vary from 0.05 to 0.2 and we pick $A_m = 0.1$.

Step 3: After determining the values of S_n and A_m, a few cases were run by varying S_c and G_{ab} to find the best material parameters to match the test data. The details will not be given here. The parameters obtained were $G_{ab} = 1$, $S_c = 0.7$.

Step 4: G_{ac} can be adjusted to match V_{50} (G_{ac} has minor effect on the BFD and deformation zone size). However, the G_{ac} value used in the base case is actually good for V_{50} data (within 10% for all the 3 thicknesses panel tests, the results will be given in the next section).

The E_c value in the base case is not changed since the numerical results using the value show good comparisons with the test data. The next section will show the comparisons with this set of material parameters. Of course, other sets of parameters might be obtained to get better agreements with the test data but we have not tried any others.

The material parameters normalized by the values in the base case we obtained through the parametric analysis are $S_n = 0.4$, $G_{ab} = 1$, $G_{ac} = 1$, $E_c = 1$, $S_c = 0.7$, and $A_m = 0.1$.

It is not surprising that the base values of G_{ab}, G_{ac}, and E_c do not need to change to match the test data since these parameters were carefully chosen based on our knowledge and information in the literature.

5.   Comparison with Test Data

The set of parameters obtained from the parametric study discussed in Section 4 was used in the model to compare with the test data, including V_{50} tests of 2 other thicknesses and another BFD test (panel 458A-2). These 3 tests were not used in the material model characterization; therefore, this can be regarded as model validations. The numerical results for the tests used in the model characterization were also given here for completion.

5.1 V_{50} Experiments

Numerically, the ballistic limit V_{50} is bracketed by the velocity at which the projectile perforates the panel and the velocity at which the projectile is stopped. To evaluate the V_{50}, calculations are carried out at different impact velocities. Figure 22 shows the time history of the projectile kinetic energy at different impacting velocities for 3 thicknesses of panels. All of the velocities are normalized by V_0, the V_{50} for panel of 7.8 kg/m^2 areal density. The energy is normalized by the energy corresponding to V_0. If the projectile residual energy is very small (e.g., 0.01% of initial energy), the projectile is assumed to be stopped by the panel. If the residual energy asymptotes to a large value, the projectile is assumed to perforate the panel. For example, for the Dyneema HB80 panel with 7.8 kg/m^2 areal density, the FSP perforates the panel when the impact velocity is higher than 1.028 V_0, while it is stopped by the panel when the impact velocity is less than 1.021 V_0. The V_{50} is thus bracketed between 1.021 V_0 and 1.028 V_0. More cases need to be run to decrease the range of this bracket. The calculated V_{50} will be the average of the highest velocity at which the projectile stopped and the lowest velocity at which the projectile perforated the panels, which is similar to the test method.
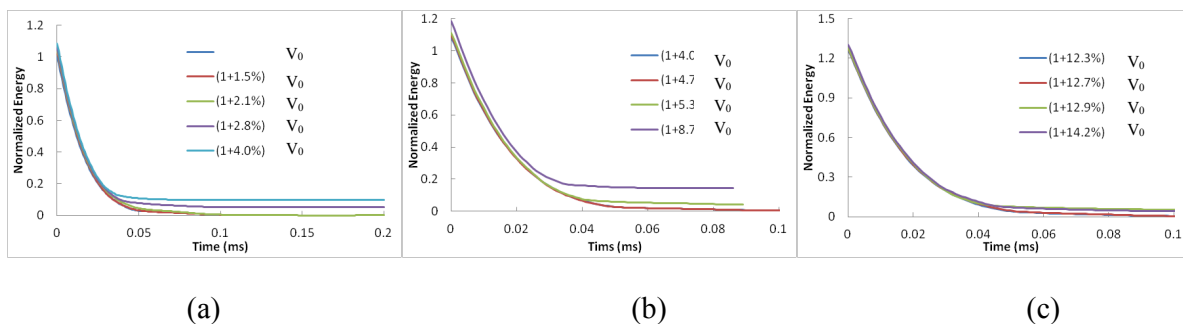

(a)   (b)   (c)

Fig. 22   Time history of projectile kinetic energy for panels with areal density of a) 7.8 kg/m^2, b) 8.8 kg/ m^2, and c) 10.7 kg/ m^2

The calculated V_{50} results are listed in Table 4 for the 3 thicknesses of panels along with the test data. The calculated V_{50} is within a 10% difference compared with the test data. The difference between the calculated V_{50} and test data increases as the panel thickness increases.

Table 4   Comparison of normalized V_{50} between tests and calculated by LS-DYNA

Areal density (kg/m²)	Tested V_{50}	Highest velocity projectile stopped	Lowest velocity projectile perforated	Calculated V_{50}	Difference (%)
7.8	1.00	1.021	1.028	1.025	2.5
8.8	1.09	1.047	1.053	1.050	−3.5
10.7	1.26	1.127	1.129	1.128	−10.4

5.2 BFD Experiments

Figure 23 shows the time history of the center BFD with previously listed parameters for the 3 BFD tests 458A-1, 458A-2, and 545A. Overall, the agreements are good. The slope of the BFD time history matches in the first stage (composite failure stage) but is slightly larger in the second stage (fiber stretch stage) given by the model. The time corresponding to the peak BFD was underpredicted in the model. The late time response does not agree well with the test data, especially for test 545A. This can possibly be improved with a better composite model accounting for strain rates effect.
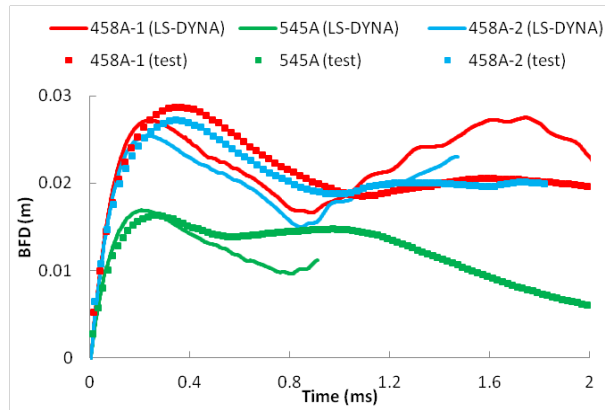
Fig. 23   Time history of center BFD for the 3 BFD tests

Figure 24 shows the damages in the panels from posttest CT scan of the UHMWPE panels and the simulation results. Only a part of the panel containing the center hit location was scanned for the 4 corners clamped test to obtain higher scan resolution. For panel 545A, full-panel scans were obtained as the resolution was found to be sufficient for full-panel scan. In both experimental and simulation results, it can be seen that a hole, similar in size to the projectile, forms around the projectile through

shearing of fibers. Many layers delaminated in the panel, with a major delamination occurring at the location where the bullet is arrested. For test 545A, the sphere rebounded. The simulation results are for the shapes corresponding to peak BFD, but the CT scan shows the final deformation. After peak BFD, the panels rebound and oscillate before equilibrium. In the model, no damping was added; as a result, the panels would not stop oscillating to attain the final shape. Therefore, it is not surprising that the peak BFD in the simulation results is larger than the final BFD in the experiments. However, the remaining thickness, extent, and nature of delamination from the simulation were close to the experimental results.

(a^1)

(a^2)

(b^1)

(b^2)

(c^1)

(c^2)
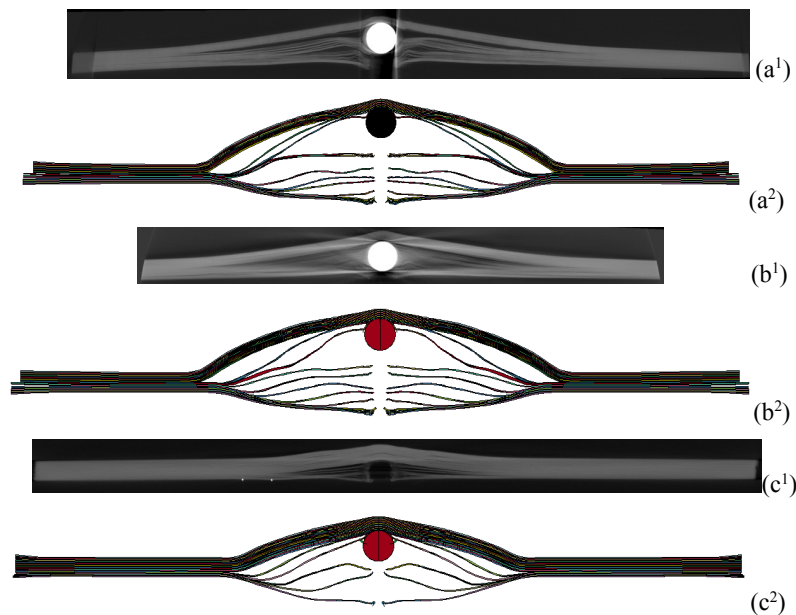
Fig. 24   Delamination in the panels for a) test 458A-1, b) 458A-2, and c) 545A (superscript 1 for CT scan from postballistic panels, superscript 2 for LS-DYNA prediction)

The deformation zone sizes are compared with the test data in Fig. 25 at 50, 100, and 200 µs (for test 545A, the DIC data was recorded every 20 µs and the results at 60, 100, and 200 µs were compared). The predicted deformation zone sizes agree well with the test data.
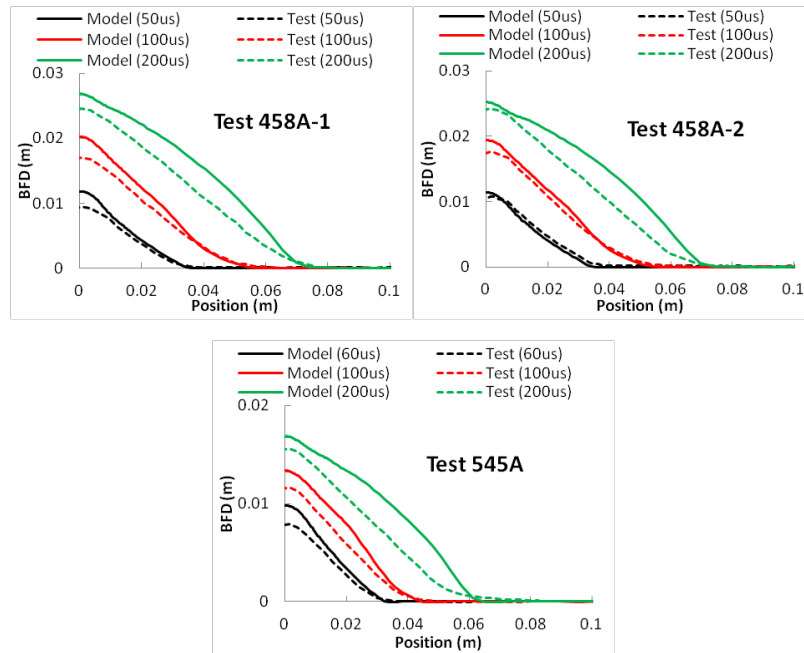
Fig. 25   Deformation zone sizes for panel 458A-1, 458A-2, and 545A.

Figure 26 shows the BFD contour for both LS-DYNA results and DIC data. For LS-DYNA, the one-quarter model results were mirrored along 2 symmetry planes to get the full model results (the vertical and horizontal lines are the 2 symmetry planes, and the black circle is the impact zone edge). For panel 545A, the DIC data are available only for half of the panel. It can be seen that the contour shapes (the center is circular but the edge is diamond) and sizes agree well, except for the smaller gradient near the center (or larger red zone) given by the model.

LS-DYNA   DIC test data
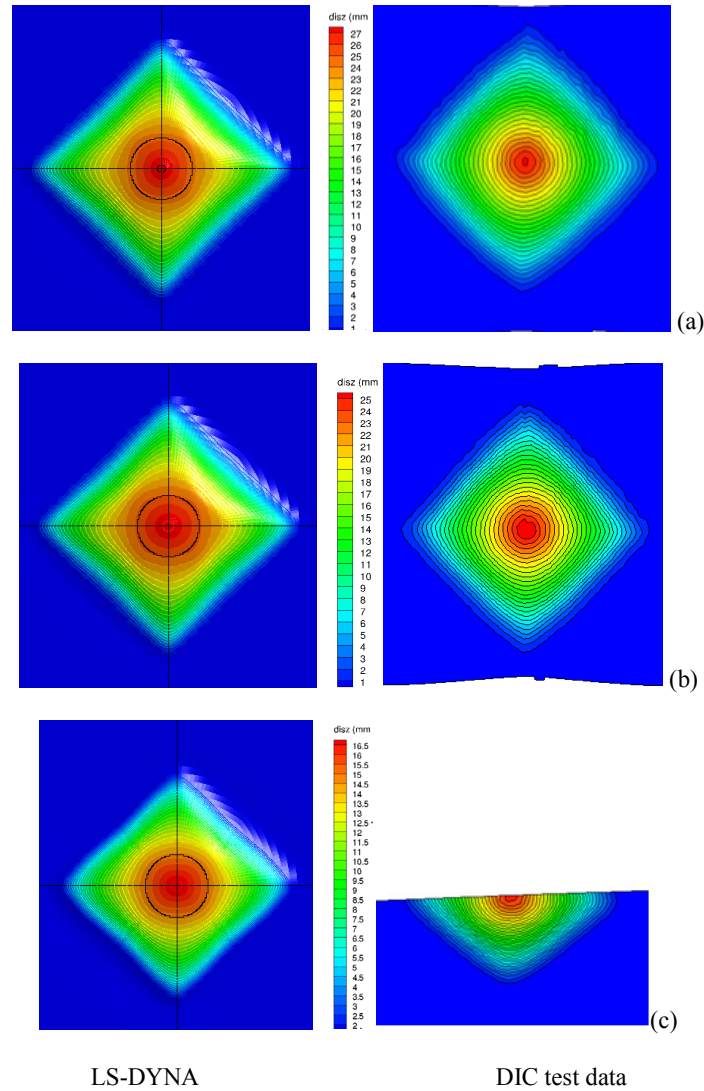
Fig. 26 BFD contour for panel a) 458A-1, b) 458A-2, and c) 545A (left is LS-DYNA results, right is DIC test data)

Table 5 compares the model predictions and test data for tests 458A-1, 458A-2, and 545A. The peak BFD predictions are within 7% difference. The thickness of the intact composite matches the test data for panel 458A-2 and 545A but is overpredicted for panel 458A-1. This could be improved if more layers are used for the panels in the numerical model, as explained previously.

Table 5   Comparison between LS-DYNA and tests

Panel/ test	Impact speed (m/s)	Peak BFD (mm)			Percent of intact composite thickness	
		LS-DYNA	Test	Difference	LS-DYNA	Test
458A-1	440.6	27.2	28.6	5.2%	45%	40.3%
458A-2	424.3	25.5	27.3	6.7%	50%	50.4%
545A	292.6	16.9	16.3	3.6%	75%	76.4%

The current model with this set of material parameters gives reasonable agreements with the test data. However, the material parameters characterized by current study are not unique. In the future, more tests need to be conducted at different impact conditions and analyzed.

6.   Conclusion

We developed a numerical model for ballistic impact response of UHMWPE composite panels based on experimental data reported earlier. Parametric studies were conducted to identify critical parameters and experimental data were used to calibrate the material model for UHMWPE. A set of material parameters was identified from the parametric analysis of ballistic experiments on UHMWPE flat plates. The simulation results with this set of parameters reasonably match the data from the experiments on ballistic limit velocity V_{50}, BFD profile, and the damage sustained by the panels, including the remaining thickness of the partially perforated composite. The last 2 measures are critical in evaluating behind helmet blunt trauma, which results when the deformed helmet contacts the head. Of course, the set of parameters is not expected to be unique but is expected to represent the composite behavior well within the calibrated ballistic parameter range. Further material tests can assist in establishing the estimated parameters and in improving the computational model. The process parameters, such as pressure and temperature, are expected to affect these material parameters. Since such data are not yet available, no conclusions can be drawn on processing condition sensitivity.

The parameter study shows the dependence and sensitivity of critical parameters, and provides guidance for improved ballistic protection. Generally, the material needs to have higher interlaminar tensile strength S_n, higher transverse Young's modulus E_c, and higher crush strength S_c, whereas smaller transverse shear modulus G_{ac} and lower damage softening parameters A_m are found to be beneficial. Larger in-plane shear modulus can lower both V_{50} and BFD, that is, the ballistic performance can be changed with the same material but different fiber orientations since various fiber orientations can enhance the in-plane shear modulus compared to [0/90] fiber orientation in agreement with experimental observations.[4]

7. References

1. Li YQ, Li XG, Gao X-L. Modeling of advanced combat helmet under ballistic impact. J Appl Mech. 2015;82(11):111004.

2. Program Executive Office Soldier. Equipment portfolio: enhanced combat helmet (ECH). 2015 Dec [accessed 2016 June 6]. http://www.peosoldier.army .mil/portfolio/#99.

3. Faux D, Garcia M, King M, Groves S, Sanchez B, Vignes R. Analysis of Dyneema panels in high velocity impacts. Livermore (CA): Lawrence Livermore National Laboratory; 2008 July. Report No.: LLNL-TR-405698.

4. Zhang TG, Satapathy SS, Vargas-Gonzalez LR, Walsh SM. Ballistic impact response of ultra-high-molecular-weight polyethylene (UHMWPE). Composite Structures. 2015;133:191–201.

5. LS-DYNA. Keyword manual, Ver. 971 R8.0. Livermore (CA): Livermore Software Technology Corporation. 2015 [accessed 2016 June 6]. http://www.lstc.com/download/manuals.

6. DSM Dyneema LLC. Dyneema high-strength, high-modulus polyethylene fiber fact sheet. Stanley (NC): DSM Dyneema LLC; 2008 Jan 1 [accessed 2016 June 6] http://www.pelicanrope.com/pdfs/Dyneema-Comprehensive-factsheet-UHMWPE.pdf.

7. Yu JH, Dehmer PG, Sands JM. The current capabilities on dynamic impact testing. Aberdeen Proving Ground (MD): Army Research Laboratory (US); 2008 July. Report No.: ARL-TR-4496.

8. Levi-Sasson A, Meshi I, Mustacchi S, Amarilio I, Benes D, Favorsky V, Eliasy R, Aboudi J, Haj-Ali R. Experimental determination of linear and nonlinear mechanical properties of laminated soft composite material system. Composites Part B. 2014;57:96–104.

9. Russell BP, Karthikeyan K, Deshpande VS, Fleck NA. The high strain rate response of ultra high molecular-weight polyethylene: from fibre to laminate. International Journal of Impact Engineering. 2013;60:1–9.

10. Heisserer U. Tensile properties of Dyneema HB plies (HB2, HB26, HB50, HB80). Geleen (The Netherlands): DSM; 2011 Jan.

11. Koh CP, Shim VPW, Tan VBC, Tan BL. Response of a high-strength flexible laminate to dynamic tension. International Journal of Impact Engineering 2008:35:559–568.

12. Iannucci L, Pope D, Dalzell M. A constitutive model for Dyneema UD. ICCM 17. Proceedings of the 17th International Conference on Composite Materials; 2009 July 27–31; Edinburgh, United Kingdom, 2009. p 10.

13. Iannucci L, Pope D. High velocity impact and armour design. Express Polymer Letters. 2011;5(3):262–272.

14. Chocron S, King N, Walker JD, Heisserer U, Werff H. Impacts and waves in Dyneema HB80 strips and laminates. Journal of Applied Mechanics. 2013; 80(3):031806.

15. Nazarian O, Zok FW. Constitutive model for the shear response of Dyneema fiber composites. Composites Part A. 2014;66:73–81.

16. Tsai CL, Guan YL, Ohanehi DC, Dillard JG, Dillard DA, Batra RC. Analysis of cohesive failure in adhesively bonded joints with the SSPH meshless method. International Journal of Adhesion and Adhesives 2014;51:67–80.

17. Zhang TG, Satapathy SS, Vargas-Gonzalez LR, Walsh SM. Experiments and simulation of ballistic impact on ultra-high-molecular-weight polyethylene (UHMWPE) flat plates. Aberdeen Proving Ground (MD): Army Research Laboratory (US); May 2014. Report No.: ARL-TR-6943.

List of Symbols, Abbreviations, and Acronyms

BFD   back-face deformation

CPU   central processing unit

CT   computed tomography

DIC   digital image correlation

FE   finite element

FSP   fragment-simulating projectile

UHMWPE   ultra-high-molecular-weight polyethylene

1 (PDF)	DEFENSE TECHNICAL INFORMATION CTR DTIC OCA	
2 (PDF)	DIRECTOR US ARMY RESEARCH LAB RDRL CIO L IMAL HRA MAIL & RECORDS MGMT	
1 (PDF)	GOVT PRINTG OFC A MALHOTRA	
7 (PDF)	NATICK SOLDIER RSRCH DEV AND ENGRNG CTR M G CARBONI M CODEGA D COLANTO R DILALLA J KIREJCZYK J PARKER J WARD	
2 (PDF)	PROG EXECUTIVE OFC SOLDIER A FOURNIER J ZHENG	
4 (PDF)	SOUTHWEST RSRCH INST C ANDERSON JR S CHOCRON T HOLMQUIST G JOHNSON	
1 (PDF)	INST FOR DEFNS ANLYS Y MACHERET	

38 DIR USARL
(PDF) RDRL SLB W
   P GILLICH
   J GURGANUS
   J IVANCIK
   W MERMAGEN
   K RAFAELS
RDRL WM
   S SCHOENFELD
RDRL WMM
   M VANLANDINGHAM
RDRL WMM A
   D O'BRIEN
   T PLAISTED
   E WETZEL
RDRL WMM B
   T BOGETTI
   B LOVE

   P MOY
   C YEN
RDRL WMM D
   S WALSH
   B CHEESEMAN
RDRL WMM E
   L VARGAS-GONZALEZ
RDRL WMP B
   A DAGRO
   A EIDSMORE
   A GUNNARSSON
   C HOPPEL
   M KLEINBERGER
   P MCKEE
   S SATAPATHY
   A SOKOLOW
   K THOMPSON
   T WEERASOORIYA
   T ZHANG
RDRL WMP C
   R BECKER
   T BJERKE
RDRL WMP D
   R DONEY
   B SCOTT
   C RANDOW
RDRL WMP E
   S BARTUS
   M BURKINS
   P SWOBODA
RDRL WMP F
   N GNIAZDOWSKI
   R GUPTA